arXiv:cond-mat/0506544v1 [cond-mat.str-el] 21 Jun 2005

Novel Orbital Ordering induced by Anisotropic Stress in a Manganite Thin Film

Y. Wakabayashi[1], D. Bizen[2], H. Nakao[2], Y. Murakami[2,3],
M. Nakamura[4*], Y. Ogimoto[5], M. Izumi[6], K. Miyano[6] and H. Sawa[1]
[1]*Photon Factory, Institute of Materials Structure Science, High Energy Accelerator Research Organization, Tsukuba 305-0801, Japan*
[2]*Department of Physics, Tohoku University, Sendai 980-8578, Japan*
[3]*Synchrotron Radiation Research Center, JAERI, Sayo, 679-5148, Japan*
[4]*Department of Applied Physics, University of Tokyo, Tokyo 113-8586, Japan*
[5]*Devices Technology Research Laboratories, SHARP Corporation, Nara 632-8567, Japan*
[6]*Research Center for Advanced Science and Technology, University of Tokyo, Tokyo 153-8904, Japan*

(Dated: March 23, 2022)

We performed resonant and nonresonant x-ray diffraction studies of a $Nd_{0.5}Sr_{0.5}MnO_3$ thin film that exhibits a clear first-order transition. Lattice parameters vary drastically at the metal-insulator transition at 170 K (= T_{MI}), and superlattice reflections appear below 140 K (= T_{CO}). The electronic structure between T_{MI} and T_{CO} is identified as *A*-type antiferromagnetic with the $d_{x^2-y^2}$ ferroorbital ordering. Below T_{CO}, a new type of antiferroorbital ordering emerges. The accommodation of the large lattice distortion at the first-order phase transition and the appearance of the novel orbital ordering are brought about by the anisotropy in the substrate, a new parameter for the phase control.

Charge ordering and orbital ordering (*CO*/*OO*) are the characteristic phenomena, which render the complex electronic phase behavior to the strongly correlated electron systems, manganites in particular[1]. A number of theoretical and experimental studies on *CO*/*OO* in $RE_{1-x}AE_xMnO_3$ (*RE*: rare earth metals; *AE*: alkali earth metals) have been conducted in the vicinity of $x = 0.5$ in order to understand the mechanism of the ordering and the resulting electronic properties [2]. Only three types of *OO* have been found dominant — one type of antiferroorbital structure (staggered arrangement of $d_{3x^2-r^2}$ and $d_{3y^2-r^2}$ orbitals, *CE*-*OO*) corresponding to *CE*-type antiferromagnetism (*AF*) and two types of ferroorbital structures ($d_{3z^2-r^2}$ and $d_{x^2-y^2}$) corresponding to *C*-type and *A*-type *AF*, respectively.

The orbital order couples intimately to the lattice distortion. One can easily envision that a tetragonal lattice distortion promotes ferroorbital structures; the compressive strain within the *c*-plane favors $d_{3z^2-r^2}$ (*C*-*OO*), while the tensile strain favors $d_{x^2-y^2}$ (*A*-*OO*). In fact, the phase control of ferroorbital ordering was achieved by manipulating the tetragonal lattice parameters employing a thin-film technique fabricated on (001) substrates[3]. In contrast, the antiferroorbital ordering inevitably involves the in-plane anisotropy and no effective means for its control has been available thus far.

Thin manganite films on (011) substrates[4] were recently found to exhibit a variety of clear first-order phase transitions[5, 6], which has not been possible in those on (001) substrates that studied extensively[7, 8, 9, 10]. From the transport and magnetic properties of these films, the antiferroorbital order has been anticipated in them, although the direct evidence of the *OO* as well as the knowledge of the *OO* structures in these films, which affect the magnetic and/or electronic properties, were lacking. In this Letter, we present results of synchrotron x-ray diffraction measurements on a $Nd_{0.5}Sr_{0.5}MnO_3$ thin film grown on $SrTiO_3$ (011). A novel antiferroorbital structure has been identified. We clearly demonstrate a new handle to manipulate the *OO*, the *anisotropic* stress.

The x-ray diffraction experiment was carried out at BL-4C and BL-16A2 of the Photon Factory, KEK, Japan. The beamlines are equipped with standard four-circle diffractometers connected to closed-cycle refrigerators. Epitaxial films were grown by the pulsed laser deposition method[5, 6]. The thickness of the sample was 80 nm. Figure 1 shows the temperature dependence of the resistivity of $Nd_{0.5}Sr_{0.5}MnO_3$ thin films grown on $SrTiO_3$ (001), (011), and (111) substrates along with that of bulk $Nd_{0.5}Sr_{0.5}MnO_3$. The film on the (011) substrate clearly shows the first-order insulator-metal phase transition while films on other substrates show only monotonous temperature dependence. The tran-

*Present address: Correlated Electron Research Center (CERC), National Institute of Advanced Industrial Science and Technology (AIST), Tsukuba, Ibaraki 305-8562, Japan

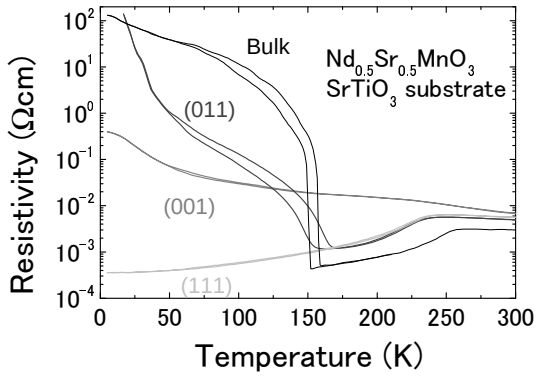


FIG. 1: Temperature dependence of the electric resistivity of $Nd_{0.5}Sr_{0.5}MnO_3$ thin films grown on $SrTiO_3$ (001), (011), and (111) substrates[6] and of bulk $Nd_{0.5}Sr_{0.5}MnO_3$[11].

sition, however, is not as sharp as that in the bulk sample and the temperature dependence of the resistivity is also different, which will be shown below to be a signature of the new *OO* in the film. It should be noted that the electronic and magnetic properties show no essential thickness dependence[5].

First, we investigated the distortion in the primitive perovskite cell. A schematic view of the a^*-plane in the reciprocal space is shown in Fig. 2(a). The lattice constants at room temperature are $a = 3.905$ Å, $b = c = 3.824$ Å, $\alpha = 90.5°$, and $\beta = \gamma = 90.3°$. As reported earlier[5, 6], the lattice constant a is locked to the substrate, while that for $[0\bar{1}1]$ is unlocked. The (002) reflection splits into four peaks at 10 K, i.e., (± 0.008, $+0.028$, $2 + 0.028$) and (± 0.008, -0.028, $2 - 0.028$). The closed circles in Fig. 2(a) show a schematic view of the reciprocal lattice at 10 K. The split along the a^*-direction is ignored as it is very small. The lattice parameters at 10 K are $a = 3.896$ Å, $b = 3.867$ Å, $c = 3.761$ Å, α=90.4°, β=90.1°, and γ=90.6°. The temperature dependence of the lattice constants during a heating run is shown in Fig. 2(b). Lattice parameters b and c vary drastically at $T_{\rm MI}$, while lattice parameter a, which is locked to the substrate, is almost constant. This freedom of lattice parameters allows the first-order transition where the resistivity rapidly changes; epitaxial films on (001) substrates are tetragonally locked and this type of distortion is suppressed. The peak profiles of a (011) line passing through the (002) position at 160 K and 180 K are shown in the inset of the figure. The profile clearly shows the phase coexistence around 160 K. The lattice parameters observed below $T_{\rm MI}$ are characterized by $a \simeq b > c$, similar to those observed in the orbital ordering in bulk manganites[12]. This feature is shared by *A-OO* and *CE-OO*, which are commonly observed in manganites in the hole concentration of $x \simeq 0.5$[13]. Therefore, the temperature dependence of the lattice parameters suggests that *A-OO* or *CE-OO* is established below $T_{\rm MI}$.

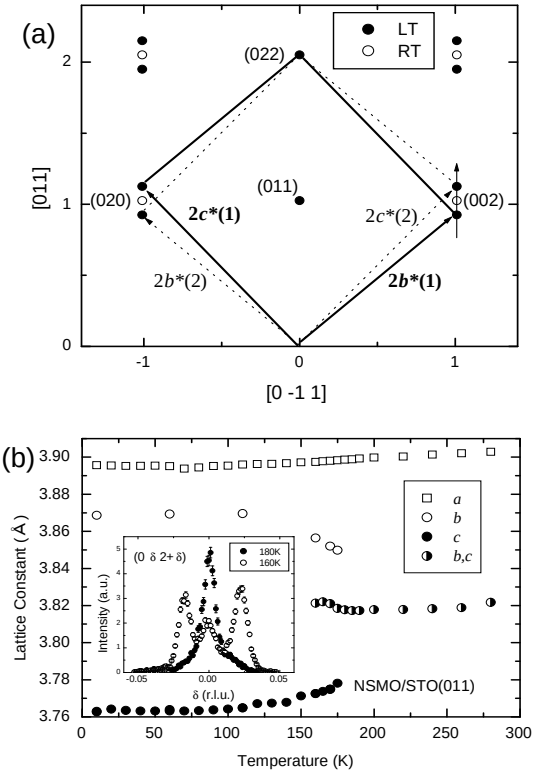


FIG. 2: (a) Schematic view of the a^*-plane in reciprocal space at room temperature and 10 K. Twinning was observed at 10 K. (b) Temperature dependence of the lattice parameters a, b, and c. The lattice parameter of $SrTiO_3$ is shown as a because a was locked into the lattice parameter of the substrate that can be measured precisely. The inset shows the peak profiles obtained at 180 K and 160 K along the arrow through (002) shown in (a).

Next, we searched for superlattice reflections corresponding to the orbital ordering. Superlattice reflections characterized by the wavevector $(\frac{1}{2}\frac{1}{2}\frac{1}{2})$ are observed at room temperature. These reflections are caused by the MnO_6-octahedra rotation and the concomitant displacement of A-site (Nd and Sr) ions. At 10 K, the intensity of these reflections differs from that observed at room temperature, indicating that the magnitude of the MnO_6-octahedra rotation changes with the phase transition. In addition, the superlattice reflections characterized by the wavevectors $(\frac{1}{4}\frac{1}{4}\frac{1}{2})$ and $(\frac{1}{2}\frac{1}{2}0)$ were observed at this temperature. The size of the unit cell at 10 K is $\sqrt{2}\times 2\sqrt{2}\times 2$ times the primitive perovskite cell, which is the same as that of the bulk compounds exhibiting *CE-OO*. The wavevector of $(\frac{1}{2}\frac{1}{2}0)$ is identical to that of the charge ordering in many bulk compounds.

The inset of Fig. 3(a) shows the intensity distribution around $(\frac{3}{4}\frac{7}{4}\frac{3}{2})$ at 10 K and 280 K. Clearly a new peak emerges at low temperatures. The intensity of this reflection as a function of temperature is shown in Fig. 3(a). The peak appears at 140 K ($= T_{\rm CO}$) during the cooling run. This temperature is significantly lower than $T_{\rm MI}$

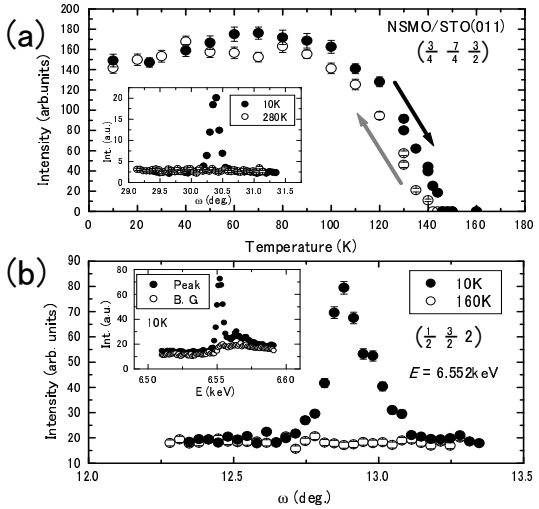


FIG. 3: (a) Temperature dependence of $(\frac{3}{4}\frac{7}{4}\frac{3}{2})$ intensity measured using incident x-rays of 6.5 keV, *off-resonant* energy. The open and closed circles indicate the results of cooling and heating run, respectively. The inset shows the intensity distribution around $(\frac{3}{4}\frac{7}{4}\frac{3}{2})$ at 10 K and 280 K. (b) Intensity distribution around $(\frac{1}{2}\frac{3}{2}2)$ measured using incident x-rays of Mn K-edge energy at 10 K and 160 K. Inset shows the energy spectrum of this reflection at 10 K.

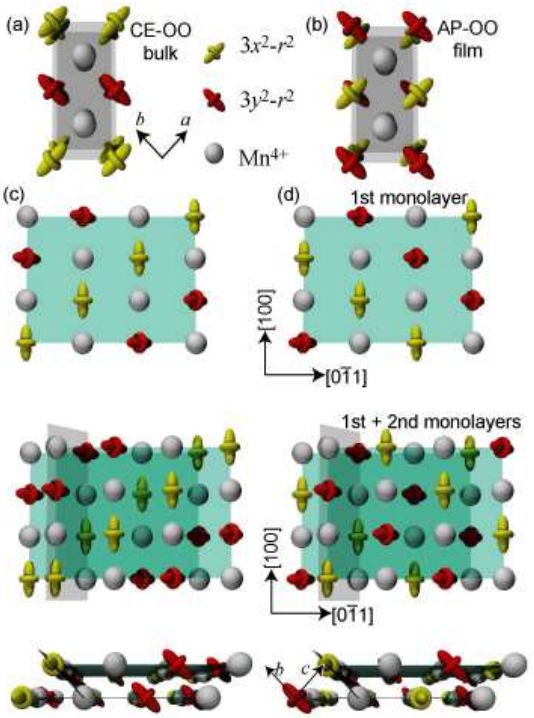


FIG. 4: (color) (a) Schematic view of the orbital arrangement in bulk compounds (*CE-OO*). The Mn^{4+} ions are indicated by white spheres, while Mn^{3+} ions with the $3x^2-r^2$ ($3y^2-r^2$) orbital are indicated by yellow (red) symbols. (b) The same as (a) but for the film (*AP-OO*). (c) The orbital arrangement of *CE-OO* observed from the [011] direction (upper two figures) and [$\bar{1}$00] direction (bottom figure). The [011] planes, which are parallel to the surface of the substrate, and the [001] planes are represented by green and gray transparent plates, respectively. (d) The same as (c) but for *AP-OO*.

at which the (002) reflection splits. We searched for superlattice reflections at 160 K, the temperature between $T_{\rm CO}$ and $T_{\rm MI}$, and found no peak except for the $(\frac{1}{2}\frac{1}{2}\frac{1}{2})$ reflections. The electronic state in this temperature region will be discussed later.

Figure 3(b) shows the peak profile of the $(\frac{1}{2}\frac{3}{2}2)$ reflection at 10 K, measured using the x-rays of Mn K-edge energy. The energy spectrum of the peak intensity at 10 K is shown in the inset. It is enhanced by a factor of 30 at the Mn K-edge. This indicates that two or more non-equivalent Mn sites form a periodic arrangement with the wavevector $(\frac{1}{2}\frac{1}{2}0)$, the ordinary charge ordering. This reflection was not observed above $T_{\rm CO}$, as shown in the figure. The temperature dependence of the intensity of this reflection is almost the same as that of the $(\frac{3}{4}\frac{7}{4}\frac{3}{2})$ reflection.

The superlattice reflections with the wavevector $(\frac{1}{4}\frac{1}{4}\frac{1}{2})$ observed at 10 K imply that the in-plane structure is the same as that of *CE-OO* with $(\frac{1}{4}\frac{1}{4}0)$ diffraction. However, the stacking pattern alternates along the c-direction. The regular *CE-OO* structure is shown in Fig.4(a). The in-plane orbital arrangement is common to systems having a variety of structure types, i.e., single-layered[14], bi-layered[15], and A-site ordered manganites[16, 17, 18], while the stacking vectors are different. Therefore, it is reasonable to expect that our film has also the same in-plane orbital arrangement. Under this assumption, we arrive at a unique solution of the orbital arrangement in the film. The result is shown in Fig. 4(b). We term this arrangement antiphase-*OO* (*AP-OO*). It is quite natural that the observed lattice parameters ($a \simeq b > c$) are similar to those found in the bulk *CE-OO* and *A-OO*.

It should be noted that the *AP-OO* must carry a magnetic structure different from that of *CE-OO*. The magnetic structure of the *AP-OO* state in the c-plane must be the same as that of the *CE-AF*, i.e., the antiferromagnetic arrangement of zig-zag ferromagnetic chains resulting from the anisotropic ferromagnetic interaction of ordered e_g orbitals. The stacking structure in the *CE-AF* is antiferromagnetic; in contrast, perfect antiferromagnetic stacking is impossible in the *AP-OO* because of the shift of the phase in the zig-zag chains in the neighboring planes. Under this constraint, two types of stacking structures are possible: the neighboring Mn^{3+} spins in the c-direction are parallel and Mn^{4+} spins antiparallel or vice versa. In both cases, lines of inter-plane transfer thread through the c-planes resulting in a unique network structure. This structure is consistent with nearly isotropic but slightly enhanced electric conductivity in the [0$\bar{1}$1] direction[5].

The *AP-OO* has not been observed in the bulk com-

pounds thus far. The novel orbital arrangement is evidently stabilized by the strain from the substrate. For a given zig-zag pattern in the c-plane, the orbital arrangement within a [011] plane in *CE-OO* and that in the *AP-OO* are identical except for the rotation of 180° about the a-axis. This is shown in the upper sectors of Figs.4 (c) and 4 (d), which indicate the first monolayers on the $SrTiO_3$ (011) substrates. Thus, the energy difference must come from the effect of the second monolayer. The second layer structures are shown in the middle and lower sectors of Figs. 4 (c) and (d). For *CE-OO*, the stress exerted by the film on the substrate is non-uniform, because the locally distorted primitive perovskite cells stack up in phase. On the other hand, the stress in the *AP-OO* is evenly distributed within the [011] plane since the arrangement is staggered. This difference can produce the energy gain of the *AP-OO* arrangement. It should be stressed that a uniquely defined crystallographic axis, as is demonstrated here, is of great importance for the study of macroscopic anisotropic properties and can be rarely achieved in bulk single crystals[19].

The stacking structure of the orbital ordering may also be affected by the distortion of the A-site ions through the hybridization of A-site ions and oxygens[20]. Since the unit cells of the film are strained by the substrate, the magnitude of the displacement of the A-site ions should differ from that of the bulk compound. This may change the stacking structure of the orbitals. However, detailed theoretical calculations of some orbital arrangements as a function of the A-site displacement has been carried out only for $x = 0$[20]. Theoretical attention for $x = 0.5$ is needed for detailed analysis.

Finally, we discuss the electronic state of the film between T_{CO} and T_{MI}. As mentioned earlier, the lattice parameter c is significantly smaller than the other two for this temperature range. This is the characteristic of *CE-OO*, *AP-OO*, and *A-OO*. However, *CE-OO* and *AP-OO* should produce the superlattice reflections characterized by the wavevectors $(\frac{1}{4}\frac{1}{4}0)$ and $(\frac{1}{4}\frac{1}{4}\frac{1}{2})$, which are not observed in this temperature range. Therefore, the expected orbital state is *A-OO*. Since magnetism is closely related to the orbital state, the suppression of the spontaneous magnetization below T_{MI} (the A-type antiferromagnetic state)[5, 6] is a natural consequence. The occurrence of A-type AF in this film is not surprising because the free energy of the A-type AF is similar to that of *CE-OO*, and thus that of *AP-OO* for $Nd_{1-x}Sr_xMnO_3$ system. In fact, the bulk compound with $x = 0.51$ exhibits the A-type AF below 200 K[12].

In summary, a new type of orbital ordering was observed in a thin film of $Nd_{0.5}Sr_{0.5}MnO_3$ fabricated on a $SrTiO_3$ (011) substrate. The orbital arrangement is clarified and the formation mechanism of this new orbital structure is discussed. The temperature dependence of the lattice parameters and the orbital ordered state are determined. A-type $AF/d_{x^2-y^2}$ ferroorbital order also appears at the intermediate temperature region. These results clearly show that various orbital structures can be realized in thin films, including the ones that do not appear in the bulk crystal. The anisotropic stress from the substrate is a new parameter for controlling the electronic state in addition to the ionic radii and the hole concentration.

The authors are grateful to Prof. T. Arima and Dr. J. P. Hill for fruitful discussions. This work was supported by a Grant-in-Aid for Creative Scientific Research (13NP0201) and TOKUTEI (16076207) from the Ministry of Education, Culture, Sports, Science and Technology of Japan and JSPS KAKENHI (15104006). Financial support to M. N. by the 21st Century COE Program for "Applied Physics on Strong Correlation" administered by Department of Applied Physics, The University of Tokyo is also appreciated.

[1] Y. Tokura and N. Nagaosa, Science **288** 462 (2000).
[2] Z. Fang *et al.*, Phys. Rev. Lett. **84** 3169 (2000).
[3] Y. Konishi *et al.*, J. Phys. Soc. Jpn. **68**, 3790 (1999).
[4] Note that the notation of the crystallographic axes is different from earlier reports[5, 6].
[5] Y. Ogimoto *et al.*, Phys. Rev. B **71**, 060403(R) (2005).
[6] M. Nakamura *et al.*, Appl. Phys. Lett. **86**, 182504 (2005).
[7] W. Prellier *et al.*, Phys. Rev. B **62**, R16337 (2000).
[8] Y. Ogimoto, *et al.*, Appl. Phys. Lett. **78**, 3505 (2001).
[9] A. Biswas *et al.*, Phys. Rev. B **63**, 184424 (2001).
[10] E. R. Buzin *et al.*, Appl. Phys. Lett. **79**, 647 (2001).
[11] Y. Tokura *et al.*, Phys. Rev. Lett. **76**, 3184. (1996)
[12] R. Kajimoto *et al.*, Phys. Rev. B **60**, 9506 (1999).
[13] K. Nakamura *et al.*, Phys. Rev. B **60**, 2425 (1999).
[14] Y. Murakami *et al.*, Phys. Rev. Lett. **80**, 1932 (1998).
[15] D. N. Argyriou *et al.*, Phys. Rev. B **61**, 15269 (2000).
[16] M. Uchida *et al.*, J. Phys. Soc. Jpn. **71** , 2605 (2002).
[17] T. Arima *et al.*, Phys. Rev. B **66** , 140408(R) (2002).
[18] H. Kageyama *et al.*, J. Phys. Soc. Jpn. **72** , 241 (2003).
[19] K. Tobe, T. Kimura, and Y. Tokura, Phys. Rev. B **69** 014407 (2004).
[20] T. Mizokawa *et al.*, Phys. Rev. B **60**, 7309 (1999).